ACS APPLIED MATERIALS & INTERFACES

Research Article

Cite This: ACS Appl. Mater. Interfaces 2019, 11, 17555−17562

www.acsami.org

Air-Stable and Oriented Mixed Lead Halide Perovskite (FA/MA) by the One-Step Deposition Method Using Zinc Iodide and an Alkylammonium Additive

Loreta A. Muscarella,[†,∥] Dina Petrova,[†] Rebecca Jorge Cervasio,[†] Aram Farawar,[†] Olivier Lugier,[†] Charlotte McLure,[†] Martin J. Slaman,[‡] Junke Wang,[§] Bruno Ehrler,[∥] Elizabeth von Hauff,[‡] and René M. Williams*[,†]

[†]Molecular Photonics Group, Van't Hoff Institute for Molecular Sciences (HIMS), Universiteit van Amsterdam, Science Park 904, 1098 XH Amsterdam, Netherlands

[‡]Department of Physics and Astronomy, Vrije Universiteit, de Boelelaan 1081, 1081 HV Amsterdam, Netherlands

[§]Molecular Materials and Nanosystems, Eindhoven University of Technology, P.O. Box 513, 5600 MB Eindhoven, Netherlands

[∥]Center for Nanophotonics, Institute AMOLF, Science Park 104, 1098 XG Amsterdam, Netherlands

Supporting Information

ABSTRACT: We present a one-step method to produce air-stable, large-grain mixed cationic lead perovskite films and powders under ambient conditions. The introduction of 2.5 % of Zn(II), confirmed by X-ray diffraction (XRD), results in stable thin films which show the same absorption and crystal structure after 2 weeks of storage under ambient conditions. Next to prolonged stability, the introduction of Zn(II) affects photophysical properties, reducing the bulk defect density, enhancing the photoluminescence (PL), and extending the charge carrier lifetime. Furthermore, 3-chloropropylamine hydrochloride is applied as the film-forming agent. The presence of this amine hydrochloride additive results in highly oriented and large crystal domains showing an ulterior improvement of PL intensity and lifetime. The material can also be prepared as black precursor powder by a solid−solid reaction under ambient conditions and can be pressed into a perovskite pellet. The prolonged stability and the easy fabrication in air makes this material suitable for large-scale, low-cost processing for optoelectronic applications.

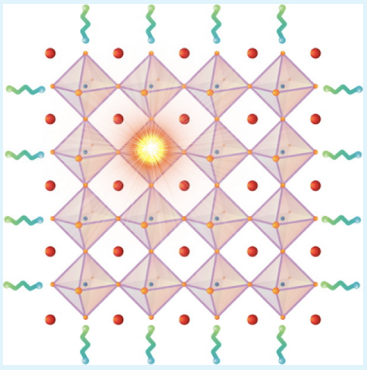

KEYWORDS: *photovoltaics, hybrid perovskite, formamidinium, methylammonium, 3-chloropropylamine chloride, zinc iodide, chloride additive*

INTRODUCTION

The rise of the power conversion efficiency (PCE) of perovskite solar cells from 3.8[1] to 24.2% in 10 years has shaken up the scientific photovoltaic community. Breakthroughs in efficiency have largely come from new strategies to fabricate perovskite thin films. Currently, improving the stability of perovskite films is a major challenge in the field.[2] Comprehensive understanding and control of the inherent photochemical properties affecting stability of these intriguing materials are therefore paramount for further progress.[3]

The chemical landscape of perovskites for solar cells is limited to basically eight main components: methylammonium (MA), formamidinium (FA), and cesium (Cs) as monovalent cations, Pb(II) and Sn(II) as divalent species and chloride, bromide, and iodide as anions. The intrinsic properties of $MAPbI_3$ and $FAPbI_3$ prohibit their use as pure materials for industrial applications such as solar cells, as they do not have suitable chemical stability due to their phase behavior.[4] $MAPbI_3$ displays a cubic to tetragonal phase transition at approximately 57 °C, and slowly turns white ($MAPbI_3{\cdot}H_2O$) or yellow ($MA_4PbI_6{\cdot}2H_2O$) when exposed to a humid atmosphere. The $FAPbI_3$ cubic black α-phase interconverts to the nonperovskite, hexagonal yellow δ-phase in a couple of weeks in dry air at RT.[5]

Significant improvements have been observed by mixing anions or cations. Incorporation of a small amount of bromide (or chloride) influences the phase changes, while the band gap remains unchanged, as already reported for $MAPbI_{2.66}Br_{0.34}$ by Weber in 1978.[6] However, chloride components in the precursor solutions tend to be mainly eliminated as HCl vapor (or as CH_3NH_3Cl) during the annealing step through an intermediate phase, if excess iodide is present (less than 1% chloride in the final phase).[7]

The most recent PCE records were obtained with (FA/MA) double (22.1 and 20.2%),[8] (FA/MA/Cs) triple (21.1%),[9] and (FA/MA/Cs/Rb) quadruple (21.6%)[10] mixed monocationic lead iodide materials.

Received: March 1, 2019
Accepted: April 16, 2019
Published: April 16, 2019

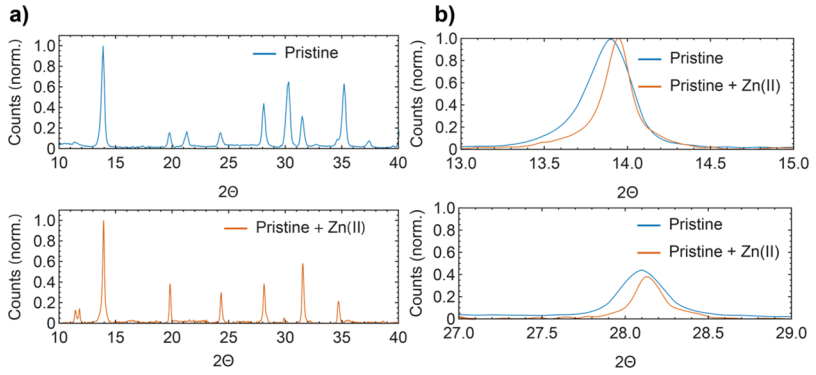

Figure 1. (a) XRD patterns of the pristine perovskite compared to the pristine containing Zn(II). (b) Magnification of the two highest diffraction peaks corresponding to (110) and (220) planes. The shift to higher 2θ indicates the incorporation of Zn(II).

So far, Sn(II) is the only divalent metal cation that can result in semiconductors of a similar band gap and electron and hole transport properties as Pb(II) equivalent, but it suffers from rapid degradation due to its chemical instability in air.[3]

Doping of traditional semiconductors is quintessential for their application in optoelectronics devices; therefore, it is tempting to dope Pb(II) perovskite thin films with various other ions. Monovalent cations Cu(I), Na(I), and Ag(I)[11] as well as Au(III), In(III), Al(III),[12] and Sr(II)[13] have been applied as dopants, and more recently Zn(II).[14−16] It has been found that for these materials, small doping levels with respect to Pb give maximum enhancement of optoelectronic properties with minimal structural modification. Furthermore, the use of additives that influence film formation[17] is of great importance. Additives with alkyl ammonium groups have been shown to influence stability of perovskite materials[18] by interacting with the perovskite crystal surface.

Here, we study the effect of Zn(II) on the photophysical properties of the mixed cations and mixed halide $(FA_{0.85}MA_{0.15})Pb(I_{2.85}Br_{0.15})$ perovskite thin films made by one-step deposition in air. In addition, we apply an amine hydrochloride additive to our perovskite, and its effect on film formation and morphology is studied. The introduction of Zn(II) results in a prolonged film stability under ambient conditions, enhanced photoluminescence (PL) and extended PL lifetime, without affecting the band gap. The main challenge for producing perovskite films from a solution is to obtain a uniform, continuous, and compact layer. For this purpose, a common and straightforward method is to apply chloride-based additives. In this study, we apply 3-chloropropylamine hydrochloride (3-CPACl) which allows to produce highly crystalline, oriented, smooth, dense, and pinhole-free layers. Furthermore, the perovskite can also be prepared from our precursors as pellet-able black powder by a solid−solid reaction under ambient conditions.

EXPERIMENTAL SECTION

Materials. Patterned indium tin oxide (ITO, 3 × 3 cm^2) with a sheet resistance of 13−15 Ω/sq was purchased from Ossila. PbI_2 (99%), ZnI_2 (98%), and 3-CPACl (98%) were purchased from Sigma-Aldrich. Methylamine hydrobromide (MABr, 98%) and Formamidine hydroiodide (FAI, 98%) were purchased from TCI. *N*,*N*-Dimethylformamide (DMF) was purchased from Biosolvie Chimie SARL.

Preparation of $(FA_{0.85}MA_{0.15})Pb(I_{2.85}Br_{0.15})$-Based Solutions. MABr (0.18 M), FAI (1.02 M) and PbI_2 (1 M) were dissolved in DMF. In order to study the effect of Zn(II), 2.5 % of ZnI_2 was also added (0.025 M). A third precursor solution was prepared including 2.5% of ZnI_2 and 2% of 3-CPACl (0.008 M) to study the effect of the amine hydrochloride additive in combination with Zn(II).

Fabrication and Characterization of Thin Films. $(FA_{0.85}MA_{0.15})Pb(I_{2.85}Br_{0.15})$ films with doping were fabricated on ITO and quartz substrates, and pure $(FA_{0.85}MA_{0.15})Pb(I_{2.85}Br_{0.15})_3$was used as a comparison. ITO and glass were cleaned by ultrasonication in water, acetone, and 2-propanol sequentially, dried with air flow, and UV−ozone treated for 30 min. Before spin coating, a N_2 flow is blown over the surface to remove dust or particles. Without the 3-CPACl additive, the precursor solution results in a yellow milky solution due to the low solubility of PbI_2 in DMF. To remove PbI_2 particles, the solution has to be filtered using a 0.2 μm syringe filter. Filtration is not necessary in the presence of the additive. Each of the solutions was spin-coated on the substrates with a speed of 4000 rpm for 30 s under ambient conditions (no acceleration factor was applied). The one-step deposition method with sprayed antisolvent (diethylether, DEE) was used. After 15 s from the start of the spin-coating programme, 0.4 mL of DEE was sprayed within ∼0.5 s over the precursor perovskite layer at a fixed height of 3 cm between the needle tip and the surface. A metal gasket from an high-performance liquid chromatography setup was used as a height fixation. After spin-coating, thin films were annealed at 100 °C for 1 h.

The stability in time of the perovskite layers was measured by monitoring UV−vis spectra and X-ray diffraction (XRD) after two weeks under ambient conditions and without encapsulation. XRD measurements were performed to investigate the introduction of Zn(II) in the perovskite lattice. The morphology and energy-dispersive system spectra of the films were characterized by using scanning electron microscopy (SEM). Steady-state PL was measured with a home-built setup equipped with a 485 nm continuous-wave laser as the source of excitation (Pico Quant LDH-D-C-640) at a power output of 1 mW. Time-correlated single-photon counting measurements were performed with a home-built setup equipped with a 485 nm pulsed laser (PicoQuant LDH-D-C-640) with a repetition rate of 0.1 MHz.

RESULTS AND DISCUSSIONS

The enhanced stability of the mixed cationic $(FA_{0.85}MA_{0.15})Pb(I_{2.85}Br_{0.15})$ perovskite compared to its single-cation and iodide-based counterparts fabricated under inert conditions was already studied before.[19] In the text, we refer to $(FA_{0.85}MA_{0.15})Pb(I_{2.85}Br_{0.15})$ as the pristine material. Here, we study the effect of the introduction of a small amount (2.5%) of the divalent transition metal Zn(II) in the abovementioned perovskite fabricated under ambient conditions. The theoretical Goldsmith tolerance factor (t) for a generic ABX_3 perovskite is calculated as shown in eq 1.

$$t = \frac{r_A + r_X}{\sqrt{2}(r_B + r_X)} \quad (1)$$

DOI: 10.1021/acsami.9b03810
ACS Appl. Mater. Interfaces 2019, 11, 17555−17562

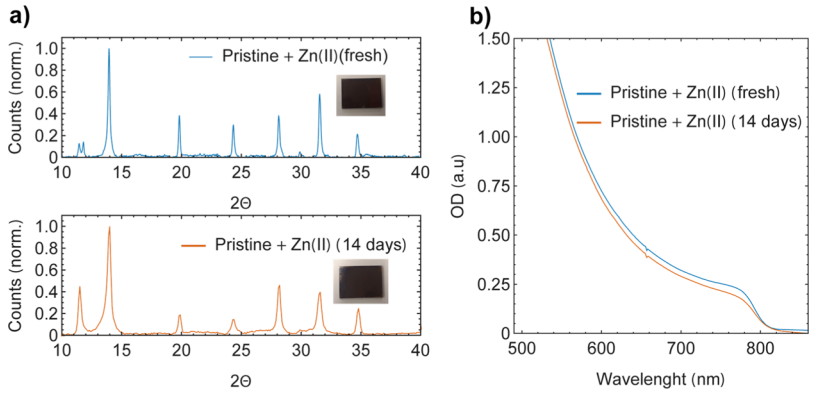

Figure 2. (a) XRD patterns of freshly made and aged pristine perovskite containing Zn(II). Inset, photographs of the fresh and aged sample are reported. (b) UV−vis absorption spectrum of the freshly made and aged pristine perovskite containing Zn(II).

Here, r_A, r_B, and r_X are the ionic radii for the cation (A), metal (B), and halide (X) sites, respectively. If the tolerance factor is in the range of 0.813−1.107, perovskites do form.[20] Weighing the contribution of the two A^+ cations and X^- anions (15:85 MA^+/FA^+ and Br^-/I^- ratio) and the two B^{2+} cations (0.025:0.975 Zn^{2+}/Pb^{2+} ratio), the resulting Goldsmith tolerance factor for the perovskite containing 2.5% Zn(II) is 0.981 compared to 0.978 for the full Pb perovskite, in agreement with the smaller ionic radius shown by Zn(II) (74 pm) compared to Pb(II) (119 pm).

The introduction of Zn (II) does not affect significantly the typical XRD pattern shown by the pristine material which results in a pseudocubic crystal structure (Figure 1a) as reported before for this material.[8] To corroborate the presence of Zn(II) in the perovskite lattice, which presumably occupies Pb^{2+} sites, the magnification of the two highest diffraction peaks is shown in Figure 1b. Both peaks show a 0.05° 2θ shift to higher values, indicating a contraction of the elementary cell in agreement with the smaller ionic radius of Zn(II). The (110) peak shifts from 13.89° to 13.94°, while the (220) peak shifts from 28.09° to 28.13°. As result, the pseudocubic lattice parameter is reduced from 6.3710 to 6.3474 Å. With Zn(II) introduction, the material shows improved crystallinity supported by the full width at half-maximum (fwhm) value reduction from 0.2799 to 0.1877.

For higher concentration of ZnI_2 (5%), UV−vis absorption measurements indicate no change in the band gap, but the XRD pattern (Figure S1) shows a stronger PbI_2 peak at 12.55° in addition to extra diffraction peaks which suggest less-oriented crystal domains and the presence of more $FAPbI_3$ δ-phase (11.47°, 21.13°, and 30.17°).[19]

ZnI_2 is a very hygroscopic salt, but it leads to higher stability against environmental moisture when introduced in our perovskite as Zn(II).

One of the causes of perovskite degradation is attributed to the oxidation of I^- to I_2 in aprotic solvent which introduces deficiency not only in I/Pb stoichiometry as reported for $MAPbI_3$ but also for other iodide-based perovskites.[21,22] For this process, moisture is essential, and the degradation is accelerated under various stresses, such as oxygen presence, light illumination, or applied bias. This degradation starts with uncontrolled incorporation of moisture during the fabrication, and for this reason, it is advisable to fabricate devices in low humidity environment. The use of a reducing agent to prevent I_2 formation was shown by Zhang et al. using hypophosphorous acid (HPA) as the additive.[23] ZnI_2, which is present in the precursor solution as Zn^{2+} and I^-, is a stronger reducing agent compared to HPA and reacts with the I_2 formed in solution during fabrication reducing defects in the stoichiometry and leading to a more stable perovskite. The reduced defect density is also reflected in the enhanced PL shown later in this work.

The stability of thin films is monitored by comparing UV−vis absorption spectra and XRD patterns of freshly made and aged films. The aged ones were measured after 14 days of storage in a Petri dish under ambient conditions of our chemical laboratory where the ambient temperature is (21.0 ± 2) °C and the relative humidity (% RH) is 40 ± 4. The pristine material starts to degrade within the first week showing a progressive color change from black (perovskite α-phase) to a complete light yellow color after 30 days (PbI_2). This degradation is confirmed by the enhancement of the PbI_2 absorption peak in the UV−vis range (∼550 nm) and the increase of the diffraction feature related to the (001) plane of lead iodide at 12° (2θ). The XRD pattern related to the aged pristine material also shows broader peaks and the presence of new diffraction peaks due to the reduced crystallinity and less oriented crystal domains (Figure S2a,b). The degradation is not reversible, and the perovskite α-phase is not recovered after reannealing. As shown in Figure 2a, the aged perovskite containing Zn(II) shows the same XRD pattern as the freshly made and a slight reduction in crystallinity, visible by the widening of the fwhm diffraction peak, which is presumably due to the interaction of the perovskite layer (not encapsulated) with the environmental humidity.

The absorption, shown in Figure 2b, does not show significant changes compared to the freshly made film. Combining these results with the visual degradation of thin films over time (inset in Figure 2a), we conclude that Zn(II) incorporation stabilizes our perovskite against environmental moisture.

A major challenge in the perovskite field is to obtain uniform, continuous, and reproducible films by spin-coating deposition with the use of antisolvents. A large number of pinholes are generated during the film formation, and long optimization processes dependent on substrates, precursor solutions, and deposition conditions are necessary before obtaining appreciable results. In recent years, many works were focused on finding tricks to circumvent this issue, and most of the time, chloride-based additives[24−26] are applied. Despite the stability improvement, our thin films suffer of pinholes and inhomogeneity as shown in the SEM image in Figure S3. As

DOI: 10.1021/acsami.9b03810
ACS Appl. Mater. Interfaces 2019, 11, 17555−17562

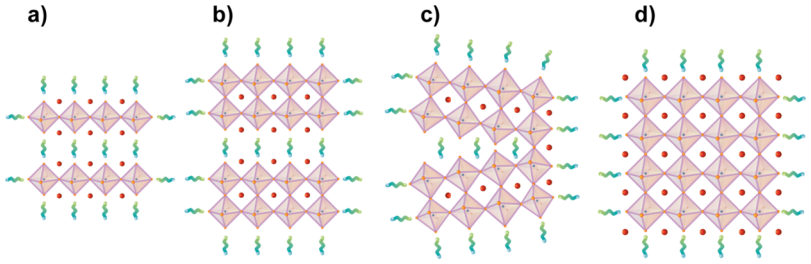

Figure 3. Proposed mechanism for additive-assisted film formation. Decreasing of the additive/perovskite ratio during spin-coating and annealing (a–c) leads to stacking of preformed crystalline units coordinated by 3-CPACl through the Pb–Cl bond resulting in an organized and compact final perovskite layer (d). The green structure represents the additive which coordinates Pb^{2+} in the perovskite unit cell.

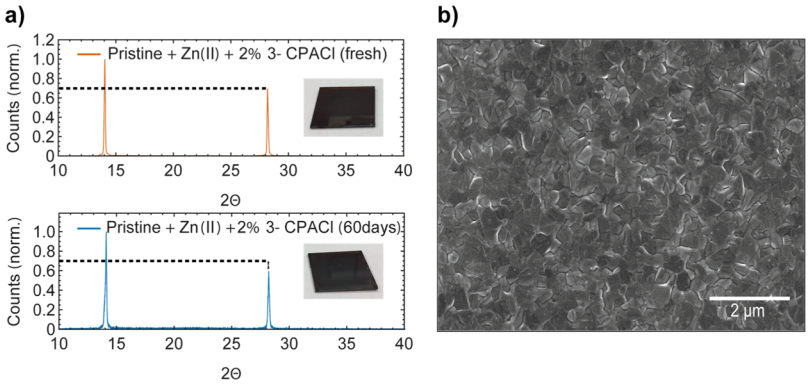

Figure 4. (a) XRD patterns of freshly made and aged perovskite containing Zn(II) and 3-CPACl. Inset: picture films before and after aging. (b) Low-magnification (20 000x) SEM image of perovskite containing Zn(II) and 3-CPACl showing a homogeneous, dense, and pinhole-free layer.

the deposition occurs under ambient conditions without control of parameters as temperature, humidity, or air-flow, it was necessary finding a straightforward method to obtain reproducible and pinhole-free layers.

We found excellent film formation with 3-CPACl, characterized by a propylic chain at whose ends an amine group and a chlorine are present. Thus, we introduce 2% of 3-CPACl in the solution of the pristine perovskite containing Zn(II). The acidic part of 3-CPACl improves solubility of PbI_2 in DMF, as also observed for other additives as HI,[27] HPA,[23] and formic acid,[28] while the chlorine bound to the propylic chain (acting as a soft Lewis base) chelates temporarily the Pb^{2+} atom (acting as a soft Lewis acid) in solution (Figure 3a), thus aiding crystals growth. We propose that a gradual change of the ratio of (FA/MA) relative to CPACl during spin-coating and annealing (Figure 3b,c) induces crystal orientation, while the additive is removed by thermal annealing, resulting in a compact and oriented layer (Figure 3d). A controlled ratio change of similar components was reported by Mitzi and co-workers with Sn(II) and *n*-butylammonium.[29]

Deposition of precursor solution containing Zn(II) and 3-CPACl results in dark brownish films immediately after spin-coating, as indicated in Figure S4 which displays a highly smooth and reflective film with full surface coverage. It is worthwhile to mention that pure MA/FA–Pb–I_xBr_y only turns black upon thermal annealing.

As shown in Figure 4a, the 3-CPACl additive induces crystal orientation and a highly oriented and stable pseudocubic structure as only the specific diffractions corresponding to (100) and (200), at 14.04° and 28.24°, remain. To estimate the crystallite sizes, the Scherrer equation was applied to the most intense peak (100) in the XRD pattern. The average crystallite size in the pristine perovskite in the perovskite containing Zn(II) and in the one containing Zn(II) and treated with 3-CPACl was found to be 36, 54, and 114 nm, respectively, indicating enlargement in size of the perovskite crystallites.

To support the role of 3-CPACl in the crystal growth, the pristine material containing only the film-forming agent reveals an average crystallite size of 87 nm, which is almost three times the crystallite size of the pristine material. A detailed summary of the calculated fwhm and crystallite size for the different materials is reported in Table S1. It is important to note that the Scherrer equation gives a rough estimation of crystallite size and is only valid for particles smaller than 0.1 μm.

To strengthen the role of 3-CPACl as a film-forming agent, Figure 4b shows the SEM image of a typical layer containing Zn(II) and treated with 3-CPACl deposited on ITO. The SEM image indicates a dense, homogeneous, and pinhole-free layer. High-resolution images of our films show ~500 nm perovskite grains (Figure S5). We note that apparent grain boundaries in the SEM do not necessarily represent crystal grain boundaries but could be purely morphological. The SEM images are thus not contradicting the grain size extracted from XRD.

To verify if the prolonged stability shown by the pristine perovskite containing Zn(II) is also maintained in the presence of 3-CPACl, UV–vis absorption spectra (Figure S6) and XRD (Figure 4a) patterns of freshly made and aged films are collected. The aged samples were measured after 60 days of storage in a Petri dish under ambient conditions of our chemical laboratory where the ambient temperature is (21.0 ± 2) °C and the relative humidity (% RH) is 40 ± 4.

Also, our Zn(II)-doped spin-coated films made with the 3-CPACl additive remain in its α-phase even after 60 days under ambient conditions. We correlate the prolonged stability under

DOI: 10.1021/acsami.9b03810
ACS Appl. Mater. Interfaces 2019, 11, 17555–17562

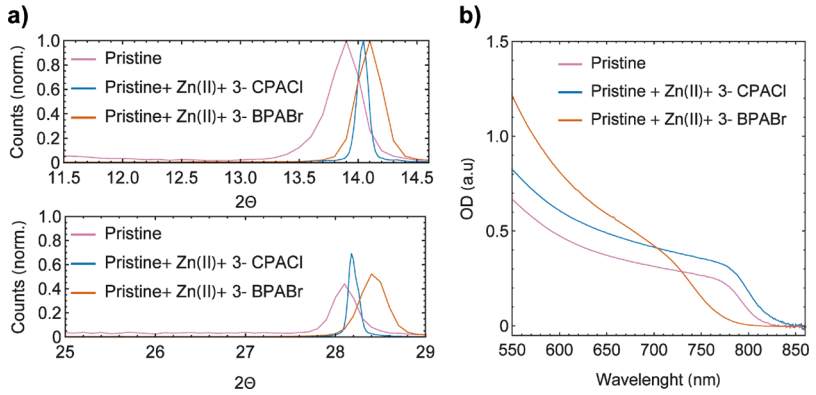

Figure 5. (a) XRD pattern magnification for the (100) and (200) of the pristine material, pristine containing Zn(II) and 3-CPACl, and the one containing Zn(II) and 3-BPABr. (b) UV−vis of the pristine material, the perovskite containing Zn(II) and treated with 3-BPABr and 3-CPACl.

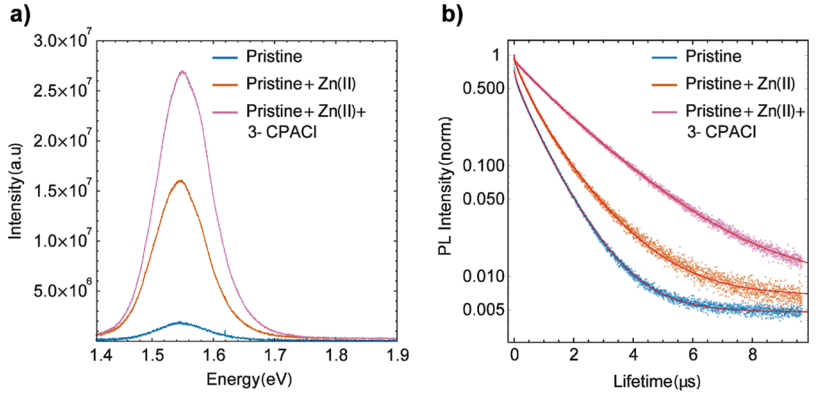

Figure 6. (a) Steady-state PL of the three compositions explored. The excitation wavelength used is 485 nm. (b). Time-resolved PL decay of the three compositions used with a excitation wavelength at 485 nm and 0.1 MHz excitation frequency.

ambient conditions to the combined action of the two additives: the preferential orientation and the grain enlargement induced by the film-forming agent reduces the amount of dangling bonds usually present at the grain boundaries, while the presence of Zn(II) can passivate Pb^{2+} vacancies and reduce the amount of I^- vacancies by striking the conversion of I^- to I_2 in the precursor solution.

After 60 days, the fwhm is slightly increased from 0.09315° ± 0.0004° to 0.1956° ± 0.0004°, while the ratio between the (100) and (200) diffraction peaks in the freshly made and in the aged sample is maintained. The Δ(fwhm) between the fresh and the aged sample is 0.1612° in the case of the pristine material containing only Zn(II), and it is reduced to 0.10245° when 2% of 3-CPACl is also applied.

As result of these findings, we can confirm that the prolonged stability is preserved and improved when ZnI_2 is used in combination with 3-CPACl.

Although energy-dispersive X-ray (EDX) analysis clearly shows the presence of Zn, Br, Pb, and I (Figure S7), we find no evidence of Cl. If the chloride not bound to the propylic chain of the additive is introduced in the material, its amount is below the detection limit of the EDX. As reported also by other works, the chloride introduced to perovskite as the additive or dopant often disappears during perovskite formation as HCl or MACl.[30]

However, a magnification of pristine and the material containing Zn(II) and 3-CPACl diffraction patterns (Figure 5a) show a shift toward higher 2θ values (14.04°), indicating a contraction of the primitive cell to 6.3027 Å which can be related to the incorporation of chloride in I^- sites. A summary of the lattice parameters reported in the text is shown in Table S2.

The use of a very similar amine hydrobromide additive (3-BPABr = 3-bromopropylamine hydrobromide) results in a highly oriented film which shows the same preferential orientation along the (100) and the (200) plane shown using 3-CPACl. This corroborates the role of the propylic chain bound to a halide atom into the crystal growth. Diffraction peaks show a shift to higher 2θ values for the perovskite treated with 3-BPABr. In particular, (100) diffraction shifts from 13.89° to 14.09°, and (200) diffraction shifts from 28.09° to 28.29°, and the lattice parameter decreases to 6.2783 Å (Figure 5a). This finding is also confirmed by the strong shift of the band gap to higher energy, indicating the incorporation of the bromide in the lattice as shown in Figure 5b. The absorption edge of our perovskite containing Zn(II) and 3-CPACl is around 830 nm, in agreement with FA/MA Pb-based perovskite mostly containing FA and iodide. The absorption in the 750−830 nm region shows a significant enhancement, and we assume that the perovskite surface morphology and coverage induced by the presence of the film-forming agent play an important role in it.

For completeness, in Figure S8, we report UV−vis and XRD measurements of freshly made and aged pristine perovskites treated with only the film-forming agent 3-CPACl. As shown, the resulting film is highly oriented along the (100) and (200) plane and 6.3027 Å as the lattice parameter which implies a contraction of the unit cell. In terms of stability, the material

DOI: 10.1021/acsami.9b03810
ACS Appl. Mater. Interfaces 2019, 11, 17555−17562

containing only 3-CPACl is stable after 60 days of exposure at ambient conditions, but it is only with a combination of the two additives that better results are achieved.

The stable, doped perovskite containing Zn(II) and 3-CPACl can alternatively be fabricated by a solid−solid reaction. The solid−solid reaction by grinding also works for other perovskite materials[31] (without additives or dopants) and pressing these materials into pellets[32] (or perovskite wafers)[33] has been applied before. Mixing the precursor components (PbI_2, FAI, MABr, ZnI_2, and CPACl) in a vial by shaking induces the reaction turning the material partly brown/black. The reaction can be completed by grinding in a marble mortar under ambient conditions, yielding a black material (Figure S9). This indicates that the perovskite α-phase is thermodynamically favorable for this composition, also in agreement with the phase stability that we observe for the final perovskite. By using a simple KBr press, the material can be turned into a perovskite pellet (see SI for procedure) that can undergo the same annealing procedure as the thin films.

We use the steady-state PL intensity to study the optical quality of our films and correlate the introduction of Zn(II) and 3-CPACl with photophysical properties of the film. PL data are normalized for the fraction of absorbed photons at 485 nm (excitation wavelength) to account for any differences in the absorption of the materials at that excitation wavelength. Relative to spin-coated layers of pristine perovskite made and measured under the same conditions, the emission intensity of the films containing Zn(II) incorporation is dramatically enhanced by an order of magnitude and including 2% of 3-CPACl, the intensity is even more boosted (Figure 6a and Table S2 for details). This implies that nonradiative recombination in the perovskite layer has been significantly suppressed.

In addition, the PL peak position set at 1.55 eV does not show a substantial shift for all the compositions except for the one containing only the film-forming agent 3-CPACl which shows a peak at 1.56 eV. Although it is not a significant shift, this might be due to the presence of a small amount of chloride in the crystal lattice. The improved stability, as a result of noteworthy improvement of the quality of the films obtained, is reflected in the photophysical properties as well.

Time-resolved PL (TRPL) was carried out to elucidate how the charge carrier dynamics of the pristine material changes with the introduction of Zn(II) and 3-CPACl. The samples were excited with a 485 nm pulsed laser with a repetition rate of 0.1 MHz. TRPL decay traces are fitted using a stretched monoexponential function $f(t) = y_0 + \sum A_i \, e^{-(t/\tau_1)^{\beta}}$ where A_i is the amplitude, τ_1 is the time constant, and β is the stretch factor ranging between 0 and 1. Our motivation to apply a stretched monoexponential function to these decays is that this model is appropriate to describe the decay in heterogeneous materials, showing monomolecular recombination distributions which have already been observed not only in spatially resolved PL works for $MAPbI_3$ films[34−36] but also for $MAPbBr_3$.[37] Such effects can be induced by differences in local material properties. Although the origin of these heterogeneities and their effects on charge dynamics are still unknown, this is beyond the scope of our work.

The lifetime is found to be 588 ns for the pristine material, 634 ns when only Zn(II) is incorporated, and 1547 ns when the film-forming 3-CPACl is applied in addition to Zn(II). This behavior is in agreement with the passivation mechanism of defects.

Point defects such as vacancies ($V_{B^{2+}}$, V_{A^+}, and V_{X^-}) and interstitials are dominant defects in ABX_3 perovskite.[38] Zinc(II) has a smaller ionic radius compared to Pb(II) and, as it is incorporated in the crystal lattice, fits in V_{Pb} or interstitial sites to passivate defects. It might also be possible that the decreases in the bulk defect density is a consequence of the increase of the formation energy of defects. Furthermore, the reduction of grain boundaries due to grain enlargement induced by 3-CPACl reduce the amount of dangling bonds, which are usually present in those regions, improving the overall quality of the film.

SUMMARY

We have shown that mixed FA/MA cations and mixed halide (Br/I) lead perovskite for solar cells, fabricated under ambient conditions, can be stabilized by the introduction of 2.5% of ZnI_2. By XRD, Zn(II) is proven to be incorporated in the perovskite structure despite its smaller ionic radius compared to Pb(II). UV−vis and XRD comparison of freshly made and aged samples containing Zn(II) show the same behavior after 14 days of storage under ambient conditions (60 days with CPACl). The incorporation of Zn(II) affects also photophysical properties of the perovskite as the PL emission is enhanced one order of magnitude in agreement with the passivation mechanism of defects and the lifetime is prolonged from 588 ns (for the pristine material) to 634 ns. In addition, to obtain dense, pinhole-free layers, we applied an amine hydrochloride additive, 3-CPACl. The introduction of this alkylammonium additive in the precursor solution results in a straightforward method to obtain reproducible and highly crystalline-oriented layers along the (100) and (200) crystallographic direction. Larger grains, homogeneous, and more compact layers are also observed in SEM images. Using Zn(II) and 3-CPACl in combination, the PL is enhanced with respect to the composition containing only Zn(II) and the lifetime extended to 1547 ns. Zn(II) is an effective isovalent dopant. The lattice contraction induced by the smaller zinc ion reduces the amount of point defects (atomic vacancies) by strain release and thereby enhances the PL lifetime. The combined effects of the alkylammonium additive and Zn(II) ions strongly reduce the amount of defect states (trap states that induce PL quenching and non-raditive charge loss in devices). We want to highlight the intriguing effect of including a transition metal as Zn(II) in the perovskite lattice also for perovskite fabricated under ambient conditions. Further work is needed to optimize the device interfaces and architecture to obtain more efficient solar cells under ambient conditions. We are optimistic that the one-step fabrication in air, together with the excellent stability enhanced by incorporation of Zn(II) and 3-CPACl, will spark these optimization efforts. A review on the effects of Zn(II) in perovskites is now available.[39]

ASSOCIATED CONTENT

Supporting Information

The Supporting Information is available free of charge on the ACS Publications website at DOI: 10.1021/acsami.9b03810.

Images of the sample containing Zn(II) and 3-CPACl during spin-coating deposition; UV−vis and XRD measurements of pure $(FA_{0.85}MA_{0.15})Pb(I_{2.85}Br_{0.15})$ and the same material containing only the hydrochloride

DOI: 10.1021/acsami.9b03810
ACS Appl. Mater. Interfaces 2019, 11, 17555−17562

additive; XRD of the film containing 5% of Zn(II); solid−solid reaction completed by ambient grinding; EDX spectrum of the film containing Zn(II) and 3-CPACl; XRD of the film containing Zn(II) and 3-CPACl on PEDOT:PSS; SEM image for the pristine material and the one containing only $Zn(II)_3$; table with crystallite sizes for each composition; and table with PL data for each composition (PDF)

AUTHOR INFORMATION

Corresponding Author

*E-mail: R.M.Williams@uva.nl.

ORCID

Loreta A. Muscarella: 0000-0002-0559-4085
Dina Petrova: 0000-0002-6682-0760
Bruno Ehrler: 0000-0002-5307-3241
Elizabeth von Hauff: 0000-0002-6269-0540
René M. Williams: 0000-0002-9490-6182

Notes

The authors declare no competing financial interest.

ACKNOWLEDGMENTS

We thank the Erasmus + exchange program for supporting L.A.M., R.J.C., O.L., and C.M. We thank Prof. Dr. Ir. R. A. J. Janssen for solar cell research facilities, Universiteit van Amsterdam for structural support, and Hysen Drogu for graphical design in Figure 3. This work is part of the research program of the Netherlands Organisation for Scientific Research (NWO).

REFERENCES

(1) Kojima, A.; Teshima, K.; Shirai, Y.; Miyasaka, T. Organometal Halide Perovskites as Visible-Light Sensitizers for Photovoltaic Cells. *J. Am. Chem. Soc.* **2009**, *131*, 6050−6051.

(2) Polman, A.; Knight, M.; Garnett, E. C.; Ehrler, B.; Sinke, W. C. Photovoltaic Materials: Present Efficiencies and Future Challenges. *Science* **2016**, *352*, aad4424.

(3) Stoumpos, C. C.; Malliakas, C. D.; Kanatzidis, M. G. Semiconducting Tin and Lead Iodide Perovskites with Organic Cations: Phase Transitions, High Mobilities, and Near-Infrared Photoluminescent Properties. *Inorg. Chem.* **2013**, *52*, 9019−9038.

(4) Baikie, T.; Fang, Y.; Kadro, J. M.; Schreyer, M.; Wei, F.; Mhaisalkar, S. G.; Graetzel, M.; White, T. J. Synthesis and Crystal Chemistry of the Hybrid Perovskite (CH3NH3)PbI3 for Solid-State Sensitised Solar Cell Applications. *J. Mater. Chem. A* **2013**, *1*, 5628−5641.

(5) Gélvez-Rueda, M. C.; Renaud, N.; Grozema, F. C. Temperature Dependent Charge Carrier Dynamics in Formamidinium Lead Iodide Perovskite. *J. Phys. Chem. C* **2017**, *121*, 23392−23397.

(6) Weber, D. CH3NH3PbX3, a Pb(II)-System with Cubic Perovskite Structure. *Z. Naturforsch., B: J. Chem. Sci.* **1978**, *1445*, 1443−1445.

(7) Yu, H.; Feng, W.; Fangyan, X.; Wenwu, L.; Jian, C.; Ni, Z. The Role of Chlorine in the Formation Process of "CH3NH3PbI3-xClx" Perovskite. *Adv. Funct. Mater.* **2014**, *24*, 7102−7108.

(8) Yang, W. S.; Noh, J. H.; Jeon, N. J.; Kim, Y. C.; Ryu, S.; Seo, J.; Seok, S. I. High-performance photovoltaic perovskite layers fabricated through intramolecular exchange. *Science* **2015**, *348*, 1234−1237.

(9) Saliba, M.; Matsui, T.; Seo, J.-Y.; Domanski, K.; Correa-Baena, J.-P.; Nazeeruddin, M. K.; Zakeeruddin, S. M.; Tress, W.; Abate, A.; Hagfeldt, A.; Grätzel, M. Cesium-Containing Triple Cation Perovskite Solar Cells: Improved Stability, Reproducibility and High Efficiency. *Energy Environ. Sci.* **2016**, *9*, 1989−1997.

(10) Saliba, M.; Matsui, T.; Domanski, K.; Seo, J.-Y.; Ummadisingu, A.; Zakeeruddin, S. M.; Correa-Baena, J.-P.; Tress, W. R.; Abate, A.; Hagfeldt, A.; Gratzel, M. Incorporation of Rubidium Cations into Perovskite Solar Cells Improves Photovoltaic Performance. *Science* **2016**, *354*, 206−209.

(11) Abdi-Jalebi, M.; Dar, M. I.; Sadhanala, A.; Senanayak, S. P.; Franckevičius, M.; Arora, N.; Hu, Y.; Nazeeruddin, M. K.; Zakeeruddin, S. M.; Grätzel, M.; Friend, R. H. Impact of Monovalent Cation Halide Additives on the Structural and Optoelectronic Properties of CH3NH3PbI3 Perovskite. *Adv. Energy Mater.* **2016**, *6*, 1502472.

(12) Wang, J. T.-W.; Wang, Z.; Pathak, S.; Zhang, W.; deQuilettes, D. W.; Wisnivesky-Rocca-Rivarola, F.; Huang, J.; Nayak, P. K.; Patel, J. B.; Mohd Yusof, H. A.; Vaynzof, Y.; Zhu, R.; Ramirez, I.; Zhang, J.; Ducati, C.; Grovenor, C.; Johnston, M. B.; Ginger, D. S.; Nicholas, R. J.; Snaith, H. J. Efficient Perovskite Solar Cells by Metal Ion Doping. *Energy Environ. Sci.* **2016**, *9*, 2892−2901.

(13) Pérez-del-Rey, D.; Forgács, D.; Hutter, E. M.; Savenije, T. J.; Nordlund, D.; Schulz, P.; Berry, J. J.; Sessolo, M.; Bolink, H. J. Strontium Insertion in Methylammonium Lead Iodide: Long Charge Carrier Lifetime and High Fill-Factor Solar Cells. *Adv. Mater.* **2016**, *28*, 9839−9845.

(14) Klug, M. T.; Osherov, A.; Haghighirad, A. A.; Stranks, S. D.; Brown, P. R.; Bai, S.; Wang, J. T.-W.; Dang, X.; Bulović, V.; Snaith, H. J.; Belcher, A. M. Tailoring Metal Halide Perovskites through Metal Substitution: Influence on Photovoltaic and Material Properties. *Energy Environ. Sci.* **2017**, *10*, 236−246.

(15) van der Stam, W.; Geuchies, J. J.; Altantzis, T.; van den Bos, K. H. W.; Meeldijk, J. D.; Van Aert, S.; Bals, S.; Vanmaekelbergh, D.; de Mello Donega, C. Highly Emissive Divalent-Ion-Doped Colloidal CsPb1−xMxBr3 Perovskite Nanocrystals through Cation Exchange. *J. Am. Chem. Soc.* **2017**, *139*, 4087−4097.

(16) Jin, J.; Li, H.; Chen, C.; Zhang, B.; Xu, L.; Dong, B.; Song, H.; Dai, Q. Enhanced Performance of Perovskite Solar Cells with Zinc Chloride Additives. *ACS Appl. Mater. Interfaces* **2017**, *9*, 42875−42882.

(17) Wang, Y.; Song, N.; Feng, L.; Deng, X. Effects of Organic Cation Additives on the Fast Growth of Perovskite Thin Films for Efficient Planar Heterojunction Solar Cells. *ACS Appl. Mater. Interfaces* **2016**, *8*, 24703−24711.

(18) Wang, F.; Geng, W.; Zhou, Y.; Fang, H.-H.; Tong, C.-J.; Loi, M. A.; Liu, L.-M.; Zhao, N. Phenylalkylamine Passivation of Organolead Halide Perovskites Enabling High-Efficiency and Air-Stable Photovoltaic Cells. *Adv. Mater.* **2016**, *28*, 9986−9992.

(19) Jeon, N. J.; Noh, J. H.; Yang, W. S.; Kim, Y. C.; Ryu, S.; Seo, J.; Seok, S. I. Il. Compositional Engineering of Perovskite Materials for High-Performance Solar Cells. *Nature* **2015**, *517*, 476−480.

(20) Li, C.; Lu, X.; Ding, W.; Feng, L.; Gao, Y.; Guo, Z. Formability of ABX3 (X = F, Cl, Br, I) halide perovskites. *Acta Crystallogr., Sect. B: Struct. Sci.* **2008**, *64*, 702−707.

(21) Wang, S.; Jiang, Y.; Juarez-Perez, E. J.; Ono, L. K.; Qi, Y. Accelerated Degradation of Methylammonium Lead Iodide Perovskites Induced by Exposure to Iodine Vapour. *Nat. Energy* **2016**, *2*, 16195.

(22) Niu, G.; Li, W.; Meng, F.; Wang, L.; Dong, H.; Qiu, Y. Study on the Stability of CH3NH3PbI3 Films and the Effect of Post-Modification by Aluminum Oxide in All-Solid-State Hybrid Solar Cells. *J. Mater. Chem. A* **2014**, *2*, 705−710.

(23) Zhang, W.; Pathak, S.; Sakai, N.; Stergiopoulos, T.; Nayak, P. K.; Noel, N. K.; Haghighirad, A. A.; Burlakov, V. M.; deQuilettes, D. W.; Sadhanala, A.; Li, W.; Wang, L.; Ginger, D. S.; Friend, R. H.; Snaith, H. J. Enhanced Optoelectronic Quality of Perovskite Thin Films with Hypophosphorous Acid for Planar Heterojunction Solar Cells. *Nat. Commun.* **2015**, *6*, 1−9.

(24) Williams, S. T.; Zuo, F.; Chueh, C.-C.; Liao, C.-Y.; Liang, P.-W.; Jen, A. K.-Y. Role of Chloride in the Morphological Evolution of Organo-Lead Halide Perovskite Thin Films. *ACS Nano* **2014**, *8*, 10640−10654.

DOI: 10.1021/acsami.9b03810
ACS Appl. Mater. Interfaces 2019, 11, 17555−17562

(25) Chueh, C.-C.; Liao, C.-Y.; Zuo, F.; Williams, S. T.; Liang, P.-W.; Jen, A. K.-Y. The Roles of Alkyl Halide Additives in Enhancing Perovskite Solar Cell Performance. *J. Mater. Chem. A* **2015**, *3*, 9058−9062.
(26) Chen, Y.; Zhao, Y.; Liang, Z. Non-Thermal Annealing Fabrication of Efficient Planar Perovskite Solar Cells with Inclusion of NH4Cl. *Chem. Mater.* **2015**, *27*, 1448−1451.
(27) Wang, F.; Yu, H.; Xu, H.; Zhao, N. HPbI3: A New Precursor Compound for Highly Efficient Solution-Processed Perovskite Solar Cells. *Adv. Funct. Mater.* **2015**, *25*, 1120−1126.
(28) Noel, N. K.; Congiu, M.; Ramadan, A. J.; Fearn, S.; McMeekin, D. P.; Patel, J. B.; Johnston, M. B.; Wenger, B.; Snaith, H. J. Unveiling the Influence of PH on the Crystallization of Hybrid Perovskites, Delivering Low Voltage Loss Photovoltaics. *Joule* **2017**, *1*, 328−343.
(29) Mitzi, D. B.; Feild, C. A.; Harrison, W. T. A.; Guloy, A. M. Conducting Tin Halides with a Layered Organic-Based Perovskite Structure. *Nature* **1994**, *369*, 467.
(30) Chen, Q.; Zhou, H.; Fang, Y.; Stieg, A. Z.; Song, T.-B.; Wang, H.-H.; Xu, X.; Liu, Y.; Lu, S.; You, J.; Sun, P.; McKay, J.; Goorsky, M. S.; Yang, Y. The Optoelectronic Role of Chlorine in CH3NH3PbI3-(Cl)-Based Perovskite Solar Cells. *Nat. Commun.* **2015**, *6*, 7269.
(31) Zhu, Z.-Y.; Yang, Q.-Q.; Gao, L.-F.; Zhang, L.; Shi, A.-Y.; Sun, C.-L.; Wang, Q.; Zhang, H.-L. Solvent-Free Mechanosynthesis of Composition-Tunable Cesium Lead Halide Perovskite Quantum Dots. *J. Phys. Chem. Lett.* **2017**, *8*, 1610−1614.
(32) Guerrero, A.; Garcia-Belmonte, G.; Mora-Sero, I.; Bisquert, J.; Kang, Y. S.; Jacobsson, T. J.; Correa-Baena, J.-P.; Hagfeldt, A. Properties of Contact and Bulk Impedances in Hybrid Lead Halide Perovskite Solar Cells Including Inductive Loop Elements. *J. Phys. Chem. C* **2016**, *120*, 8023−8032.
(33) Shrestha, S.; Fischer, R.; Matt, G. J.; Feldner, P.; Michel, T.; Osvet, A.; Levchuk, I.; Merle, B.; Golkar, S.; Chen, H.; Tedde, S. F.; Hock, R.; Rührig, M.; Göken, M.; Heiss, W.; Anton, G.; Brabec, C. J. HIGH-Performance Direct Conversion X-Ray Detectors Based on Sintered Hybrid Lead Triiodide Perovskite Wafers. *Nat. Photonics* **2017**, *11*, 436.
(34) Nie, W.; Tsai, H.; Asadpour, R.; Blancon, J.-C.; Neukirch, A. J.; Gupta, G.; Crochet, J. J.; Chhowalla, M.; Tretiak, S.; Alam, M. A.; Wang, H.-L.; Mohite, A. D. High-Efficiency Solution-Processed Perovskite Solar Cells with Millimeter-Scale Grains. *Science* **2015**, *347*, 522−525.
(35) Vinet, L.; Zhedanov, A. A "missingö family of classical orthogonal polynomials. *J. Phys. A: Math. Theor.* **2011**, *44*, 085201.
(36) Draguta, S.; Thakur, S.; Morozov, Y. V.; Wang, Y.; Manser, J. S.; Kamat, P. V.; Kuno, M. Spatially Non-Uniform Trap State Densities in Solution-Processed Hybrid Perovskite Thin Films. *J. Phys. Chem. Lett.* **2016**, *7*, 715−721.
(37) Vrućinić, M.; Matthiesen, C.; Sadhanala, A.; Divitini, G.; Cacovich, S.; Dutton, S. E.; Ducati, C.; Atatüre, M.; Snaith, H.; Friend, R. H.; Sirringhaus, H.; Deschler, F. Local Versus Long-Range Diffusion Effects of Photoexcited States on Radiative Recombination in Organic-Inorganic Lead Halide Perovskites. *Adv. Sci.* **2015**, *2*, 1500136.
(38) Buin, A.; Pietsch, P.; Xu, J.; Voznyy, O.; Ip, A. H.; Comin, R.; Sargent, E. H. Materials Processing Routes to Trap-Free Halide Perovskites. *Nano Lett.* **2014**, *14*, 6281−6286.
(39) Kooijman, A.; Muscarella, L. A.; Williams, R. M. Perovskite Thin Film Materials Stabilized and Enhanced by Zinc(II) Doping. *Appl. Sci.* **2019**, *9*, 1678.

DOI: 10.1021/acsami.9b03810
ACS Appl. Mater. Interfaces 2019, 11, 17555−17562